Eliminating ultraviolet optical absorption through Fe-impurity engineering: *Ab initio* study of the nonlinear optical crystal $K_2Al_2B_2O_7$

Z. S. Lin,[1] L. F. Xu,[2] Lijuan Liu,[1] J. Xu,[3] M. H. Lee,[4] Z. Fang,[2] and C. T. Chen[1]
[1]*Beijing Center for Crystal R&D, Key Laboratory of Functional Crystals and Laser Technology, Technical Institute of Physics and Chemistry, Chinese Academy of Sciences, P.O. Box 2711, Beijing 100190, China*
[2]*Institute of Physics, Chinese Academy of Sciences, P.O. Box 603, Beijing 100190, China*
[3]*Department of Physics, Renmin University of China, Beijing 100872, China*
[4]*Department of Physics, Tamkang University, Tamsui, Taipei 25137, Taiwan*
(Received 12 May 2010; revised manuscript received 3 July 2010; published 28 July 2010)

We show, based on systematic first-principles calculations, that the ultraviolet (UV) optical properties of the nonlinear optical crystal $K_2Al_2B_2O_7$ can be dramatically improved by eliminating the Fe impurity through the controlling of Fe charge state during crystal growth. Our results reveal that the Fe^{3+} impurity can easily replace the Al site with very low formation energy, resulting in the strong UV absorption which can be quantitatively understood from the formation of in-gap states and corresponding *p-d* transition. Moreover, it is demonstrated that modification of the Fe charge state greatly increases its formation energy, which prevents it from incorporation into the crystal during the growth process and results in the elimination of these absorption peaks and the improvement of UV optical properties.

DOI: 10.1103/PhysRevB.82.035124 PACS number(s): 78.20.Ci, 71.15.Nc, 71.20.−b

I. INTRODUCTION

Recent developments in medical, lithographic, spectroscopic, and optical storage applications require all-solid-state laser sources in the ultraviolet (UV) spectrum,[1–3] especially at the wavelength of 266 and 193 nm. Numerous efforts have been made to search for nonlinear optical (NLO) crystals which can produce coherent light at these wavelengths by harmonic generation efficiently.[4–9] $K_2Al_2B_2O_7$ (KABO), a newly developed NLO borate crystal, is considered to be one of the best candidates for this purpose due to its wide range of optical transparency down to 180 nm and very suitable structural characteristics for UV harmonic generation.[8,9]

However, KABO crystals obtained from the conventional top-seeded solution growth method always exhibit strong optical absorption for wavelengths in the range 190–280 nm, which significantly hinders applications of the borate in UV laser sources. Electron paramagnetic resonance analysis has demonstrated that this absorption is induced by iron impurities,[10] which are always present in the growth environment (e.g., in raw materials and/or in the chamber of the growth furnace). Actually, this optical phenomenon is so sensitive to the presence of iron impurity that trace amounts of iron impurity (in ppm) are enough to produce the UV absorption in KABO even grown from the raw materials with analytic purity (>99.99%), thus its elimination is a very difficult task. Therefore, some interesting questions arise: (i) why the iron impurity easily incorporated into the KABO crystals? (ii) what microscopic mechanism resulting the occurrence of UV optical absorption peaks in KABO containing the iron impurity? and more importantly, (iii) how to eliminate these UV absorption peaks through Fe-impurity engineering? Understanding these issues is crucial for improving the optical quality of NLO crystals. The presence of iron in some oxides, such as TiO_2 (Ref. 11) and glass (Ref. 12), also causes similar absorption phenomena, thus investigations of the KABO case would be helpful in producing other materials in good optical quality.

The structural and electronic properties of oxides with iron impurity have been extensively investigated in the frame of density-functional theory (DFT), which has proved to be very successful for the vast majority of compounds. It was found, however, that the standard LDA or GGA method fails to describe the localized states in the transition element. Therefore, an additional on-site orbital-dependent (*d* orbitals-related) correlation Hubbard *U* (Refs. 13 and 14) is usually adopted to correct this problem in the so-called LDA+*U* or GGA+*U* methods.

In this work, using the first-principles computational approaches, we systematically study the formation of iron impurity and the corresponding optical properties of KABO. Furthermore we reveal a mechanism for preventing the incorporation of iron into the crystal during the growth process. It is found that (i) the Fe impurity easily substitutes on the Al site with very low formation energy; (ii) the UV optical absorption peaks result from the electronic transition between O 2*p* states and Fe 3*d* band-gap states split by the crystal field; and (iii) modification of the Fe charge state greatly increases its formation energy, and prevents the Fe impurity from incorporating into the host lattice. This Fe-impurity engineering eliminates the UV optical absorption peaks of KABO in the experiments.

II. COMPUTATIONAL METHOD

The structure of KABO (Refs. 8 and 9) is shown in Fig. 1. It clearly shows that the nearly planar $(Al_3B_3O_6)$ networks perpendicular to the *c* axis are connected to one another by bridged oxygen atoms, and potassium cations are located between the layers. In the $(Al_3B_3O_6)$ layer each Al atom is linked with three terminal O atoms of $(BO_3)^{3-}$ groups and a bridged oxygen to form a tetrahedral $(AlO_4)^{5-}$ group.

The calculations are based on the spin-polarized plane-wave pseudopotential method[15] implemented in the CASTEP package.[16] Ultrasoft pseudopotentials[17] are used with 1*s*, 2*s*,

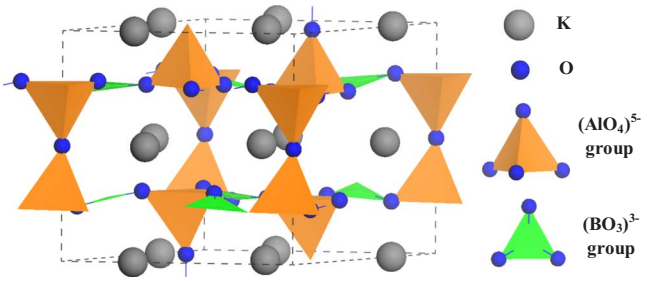

FIG. 1. (Color online) Unit cell of KABO with space group $R32$, $a=b=8.530$ Å, $c=8.409$ Å, $\alpha=\beta=90°$, and $\gamma=120°$. The grey and blue balls represent potassium and oxygen atoms, respectively. The green triangles and orange tetrahedrons represent $(BO_3)^{3-}$ and $(AlO_4)^{5-}$ groups, respectively.

and $2p$ electrons for potassium and aluminum, and the $1s$ electrons for boron and oxygen treated as core electrons. For iron, the $3d$ and $4s$ electrons are treated as the valence electrons. A kinetic-energy cutoff of 500 eV and the Perdew, Burke, and Ernzerhof functional[18] are chosen for all the calculations. A 39-atom KABO unit cell doped by a single iron atom is used to simulate a dilute iron impurity. Tests show that the calculated formation energy in this size of cell with periodic boundary conditions is accurate to about 0.1 eV compared to that in a 312-atom supercell, and thus the choice of cell size is adequate for the current studies. Brillouin-zone integrations are made using $(3\times3\times3)$ k-point meshes according to the Monkhorst-Pack scheme.[19] The supercell volume and the atomic positions for the bulk are fully optimized using the quasi-Newton method.[20] The convergence thresholds between optimization cycles for energy change, maximum force, maximum stress, and maximum displacement are set as 10^{-5} eV/atom, 0.03 eV/Å, 0.05 GPa, and 0.001 Å, respectively. The optimization terminates when all of these criteria are satisfied.

The formation energy of an iron-impurity atom in KABO is defined as[21]

$$E_f(\mathrm{Fe}) = E_{tot}(\mathrm{Fe+host}) - E_{tot}(\mathrm{host}) + n_A(\mu_A^0 + \Delta\mu_A) - (\mu_{\mathrm{Fe}}^0 + \Delta\mu_{\mathrm{Fe}}), \quad (1)$$

where E_{tot}(Fe+host) is the total energy of a KABO unit cell containing a single Fe atom and E_{tot}(host) is the total energy of a perfect KABO unit cell. n_A is the number of atoms removed during the defect formation from the host crystal to the atomic reservoir, i.e., $n_A=1$ for the A atom (A=K, Al, B, or O) which is replaced by an iron atom and $n_A=0$ for an interstitial iron impurity. $\Delta\mu_A$ is the chemical potential with respect to the GGA energy μ_A^0 of the elemental solid A (for oxygen, μ_O^0 is the energy per atom of an O_2 molecule) and varied to the O-rich condition with the production of oxide A_mO_n. However, the chemical potential of the A atom in the oxide phase is not straightforward to evaluate. One approach is to consider the chemical potential of the A atom to be a function of the oxygen chemical potential by

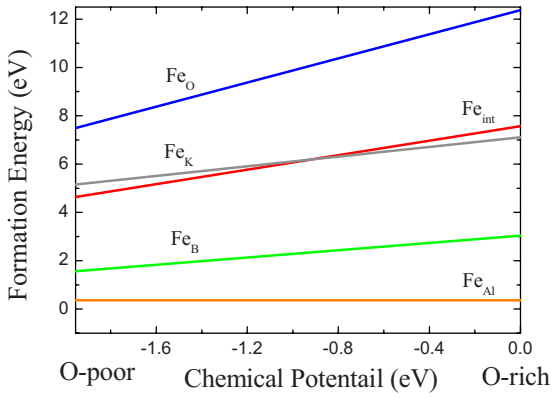

FIG. 2. (Color online) Formation energies of the single iron impurity in KABO as a function of oxygen chemical potential μ_O. Fe_O, Fe_K, Fe_{Al}, and Fe_B represent iron atom substitutions into O, K, Al, and B sites, respectively, and Fe_{int} represents the interstitial iron impurity.

$$\Delta\mu_A = \frac{\Delta H_f(A_mO_n) - n\Delta\mu(\mathrm{O})}{m}, \quad (2)$$

where $\Delta H_f(A_mO_n)$ is the calculated formation enthalpy for oxide A_mO_n. The oxygen chemical potential must vary in the energy range

$$\max[1/n\Delta H_f(A_mO_n)] \le \Delta\mu_O \le 0 \quad (3)$$

otherwise, bulk A_mO_n would be precipitated from the host lattice.

Since KABO is synthesized by the following reaction:[22]

$$K_2CO_3 + Al_2O_3 + B_2O_3 \rightarrow K_2Al_2B_2O_7 + CO_2\uparrow \quad (4)$$

K_2O, Al_2O_3, and B_2O_3 are used to determine the respective chemical potentials of the A atoms under the O-rich condition. For the chemical potential of iron, the most commonly occurring oxide Fe_2O_3 is chosen as a source for the calculations.

III. RESULTS AND DISCUSSION

A. Formation of Fe impurity

Figure 2 shows the formation energies for an iron-impurity atom incorporated into the various sites of the KABO cell, as a function of the ambient oxygen chemical potential. It is clear that Fe substituted on an O site (Fe_O) has the highest formation energy while its substitution on an Al site (Fe_{Al}) gives the lowest formation energy over the entire range of oxygen chemical potential. This means that the Fe_{Al} impurity is the one most likely to form in KABO compared to the others, and this can also be understood by the fact that the ionic radius of Al^{3+} (1.26 Å) is very similar to that of Fe^{3+} (1.27 Å). Furthermore, the lower Fe_{Al} formation energy 0.32 eV makes it replace Al site with high probability in the growth temperature about 1100 K (Ref. 22) ($k_BT\sim0.1$ eV) for KABO. Therefore KABO crystals obtained under conventional growth conditions are easily doped with Fe_{Al} impurity.

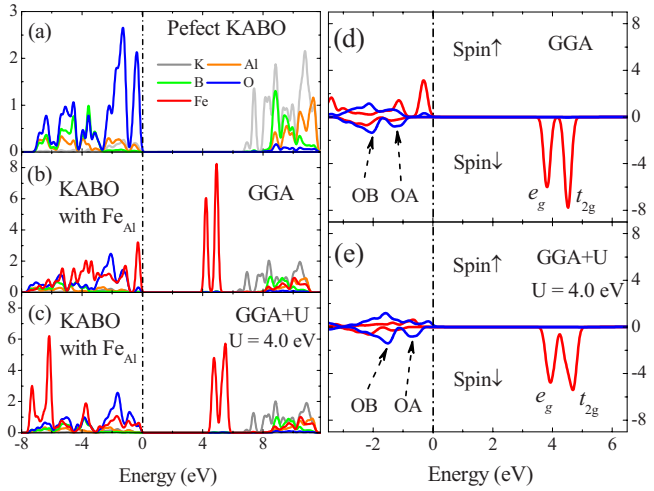

FIG. 3. (Color online) PDOS projected on each species of atoms with the band-gap correction in the perfect and Fe_{Al}-doped KABO. (a) Perfect KABO, (b) Fe-doped KABO with GGA, and (c) Fe-doped KABO with GGA+U. The corresponding orbital-resolved spin-polarized PDOS on oxygen $2p$ orbitals and iron $3d$ orbitals are plotted in (d) and (e), respectively. The straight dashed dotted lines indicate the VBM. Note that the ratio of the number of oxygen and iron atoms is 21:1 in a KABO supercell.

B. Electronic properties

The partial densities of states (PDOS) for KABO with and without the Fe_{Al} impurity are shown in Fig. 3, in which only the top of the valence band (VB) and the bottom of conduction band (CB) are shown, since the optical absorption characteristics of KABO in the UV spectrum are mainly determined by the states close to the band gap. For perfect KABO [Fig. 3(a)], the top part of the VB from −4 to 0 eV are mainly composed of O $2p$ orbitals and the K $4s$ orbitals are located at the bottom of the CB. When the Fe_{Al} impurity forms in KABO, the impurity-induced defect states (IIDS) in the band gap are split into two peaks [Fig. 3(b)]. The detailed spin-polarized PDOS analysis [Fig. 3(d)] shows that those IIDS are generated by the Fe $3d$ spin-down orbitals exclusively. However, the GGA calculation shows that some Fe $3d$ spin-up orbitals accumulate unphysically at the VB maximum (VBM) and push the O $2p$ orbitals downward to lower energy. In order to correct this problem, the GGA+U method[23] is employed by explicitly adding an additional on-site Coulomb interaction, Hubbard potential U, to the Hamiltonian. The improved PDOS (U=4.0 eV for the iron $3d$ orbitals) for the Fe-doped KABO is shown in Fig. 3(c), and the spin-polarized PDOS for O $2p$ and Fe $3d$ orbitals in Fig. 3(e). Using GGA+U the Fe $3d$ spin-up orbitals located at the VBM move downward, and, in turn, the VBM are mainly composed of the O $2p$ spin-up orbitals. Our further calculations show that, in fact, this physical feature is essentially same with respect to the variation of U values from 2 to 8 eV in this system. The spin-down electronic bands, on the other hand, are insensitive to the Hubbard potential.

The splitting of IIDS observed in the electronic band structures can be explicitly understood using crystal-field theory. As a Fe atom substitutes on the Al site in KABO, it bonds to the neighboring four oxygen atoms and forms a $(FeO_4)^{5-}$ tetrahedral group, in which the Fe^{3+} ion has five $3d$ electrons and each O^{2-} ion has six $2p$ electrons. The calculated large energy difference between the nonmagnetic and ferromagnetic solutions and the strong spin polarization of Fe^{3+} ion suggests that the high spin configuration is favored due to the strong Hund's coupling. In addition, the tetrahedral crystal field will split the original quintuple degenerate Fe^{3+} $3d$ level into e_g (double degenerate) and t_{2g} orbitals (triple degenerate), resulting in an $e_g^{2\uparrow} t_{2g}^{3\uparrow}$ arrangement with the effective moment of 5/2. This means that their spin-down IIDS orbitals are totally unoccupied, consistent with our DFT results in Fig. 3(e). Meanwhile, the $2p$ orbitals of the O^{2-} ion are fully occupied and are located at the highest occupied states of the system. Obviously, it can be expected that the electronic transition (or optical absorption) would occur from the O^{2-} $2p$ spin-down states to the Fe^{3+} IIDS since the incident photon energy is enough. The transition involving the spin-up electron is prohibited according to the Pauli exclusion principle.

C. UV optical absorption induced from Fe impurity

Based on the electronic structures, the optical absorption spectrum can be calculated from the electronic transition between the *spin-parallel* occupied and unoccupied states caused by the interaction with photons[24]

$$\varepsilon_2(\hbar\omega) = \frac{2e^2\pi}{\Omega\varepsilon_0} \sum_{k,v,c} |\langle \psi_k^c | \hat{u} \cdot \vec{r} | \psi_k^v \rangle|^2 \delta(E_k^c - E_k^v - \hbar\omega), \quad (5)$$

where Ω is the volume of the elementary cell, v and c represent the valence and conduction bands, respectively, ω is the frequency of the incident light, and $\hat{u}$ is the vector defining the polarization of the electric field of the incident light, which is averaged over all spatial directions in the polycrystalline case. It should be noted that the band gap calculated by the GGA (or GGA+U) method, which is a ground-state theory, is, in general, smaller than the experimental data for the wide band-gap insulator. Therefore, a scissors operator[25,26] is usually introduced to shift all the conduction bands in order to agree with the measured value of the band gap, which is in the good determination of the low-energy structures in the imaginary part of the dielectric functions. With this correction the optical properties of various borate crystals have been successfully studied.[27]

The calculated optical absorption spectra of the perfect and Fe_{Al}-doped KABO are shown in Fig. 4, in which the experimental curve is also displayed for comparison. Clearly, our calculated spectra are in very good agreement with the experimental results, not only for the position but also for the relative strength of the optical absorption peaks centered at 4.7 eV (~260 nm) and 5.7 eV (~220 nm). In addition, another optical absorption peak located at about 6.5 eV (~190 nm) is also observed, which is confirmed by the experimental curve as the tail in the spectrum region higher than 6.0 eV (below 200 nm).

In order to elucidate the microscopic mechanism for the above optical observation in KABO, an optical band-resolved technique[28] is adopted to investigate the electronic

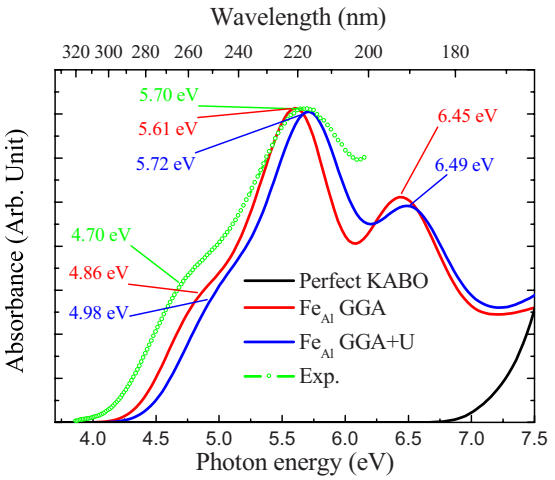

FIG. 4. (Color online) UV optical absorption spectra of KABO with the Fe_{Al} impurity. Experimental data come from Ref. 10. For comparison, the intensity of the experimental maximum at about 5.7 eV is fitted to match the maximum at the GGA curve. The curve for perfect KABO is shown at the right corner.

transition at the specified photon energy band by band. It is found that the optical absorption peaks in the UV region are completely generated from the *spin-down* electronic transition between the oxygen $2p$ states and the iron $3d$ IIDS. The electronic transition between the oxygen states centered at about 0.3 eV (indicated as OA in Fig. 3) below the spin-down VBM and the e_g and t_{2g} orbitals of the iron $3d$ states result in the optical absorption peaks located at about 4.7 eV and 5.7 eV, respectively, consistent with the above crystal-field theory consideration. Besides this contribution, another electronic transition from the oxygen $2p$ states at about 1.3 eV (OB in Fig. 3) below the spin-down VBM to the e_g and t_{2g} states corresponds to the optical absorption peaks located at about 5.7 eV and 6.5 eV, respectively. Taking account of the fact that the electronic transition energies of OA$\rightarrow t_{2g}$ and OB$\rightarrow e_g$ are in coincidence, and that the e_g and t_{2g} orbitals are doubly and triply degenerate, respectively, one can easily find that the ratio of electronic transition rates at the energies of 4.7, 5.7, and 6.5 eV is 2:5:3, consistent with the relative strength of the corresponding optical absorption peaks shown in Fig. 4.

D. Elimination of Fe impurity and UV absorption

The above formation energy calculations clearly reveal that in the conventional single-crystal growth method it is indeed very difficult to avoid the formation of the Fe_{Al} impurity in KABO. To overcome this problem, we consider that the modification of the charge state of Fe may affect the tendency of the impurity to incorporate into the Al site. Therefore, we calculate the formation energy of the charged Fe_{Al} defect for which Eq. (1) is modified to take account of the electronic contribution

$$E_f(\mathrm{Fe}) = E_{tot}(\mathrm{Fe+host}) - E_{tot}(\mathrm{host}) + n_A(\mu_A^0 + \Delta\mu_A) - (\mu_{\mathrm{Fe}}^0 + \Delta\mu_{\mathrm{Fe}}) + q(E_v + E_F), \quad (6)$$

where q is the "net" charge on the Fe ion, which is defined as the variation of the charge on the Fe ion from +3, e.g., for Fe^{2+} $q=-1$, for Fe^{4+} $q=+1$, etc. The chemical potential of the electrons, E_F, is varied from the VB maximum to the CB minimum, i.e., in the band gap (E_g) of perfect KABO. The VBM, E_v, is obtained from $E_v = E_{tot}(0,\mathrm{host}) - E_{tot}(+1,\mathrm{host})$, where $E_{tot}(0,\mathrm{host})$ is the total energy of the neutral host supercell and $E_{tot}(+1,\mathrm{host})$ is that of the +1 charged host supercell.

However, the formation energy defined by Eq. (6) is rather approximate due to the supercell model and DFT employed by our calculations, and corrections need to be included.[21,29] Here we considered two factors which have a dominant contribution to the correction: (i) the DFT band-gap correction, i.e., the difference between the GGA and experimental band gap $\Delta E_g = E_g^{\mathrm{exp.}} - E_g^{\mathrm{cal.}}$, this is required to give the proper allowed range for the electronic chemical potential, and the correction for a charged cell is given by $\Delta E_g^{\mathrm{corr}} = q\Delta E_g$; (ii) the electrostatic potential correction. The electronic chemical potential is referenced with respect to E_v of the host material, so an alignment of the potential between the supercell with the impurity and the host supercell is necessary. Namely, $\Delta V_{av}^{\mathrm{corr}} = V_{av}(\mathrm{impurity}) - V_{av}(\mathrm{host})$, where V_{av} is an average electrostatic potential within the supercell. Further energy adjustments such as the image charge correction[30] are ignored due to the improved screening of the image charge interaction in insulators.[31]

Therefore, by including the above corrections Eq. (6) becomes

$$E_f(\mathrm{Fe}) = E_{tot}(\mathrm{Fe+host}) - E_{tot}(\mathrm{host}) + n_A(\mu_A^0 + \Delta\mu_A) - (\mu_{\mathrm{Fe}}^0 + \Delta\mu_{\mathrm{Fe}}) + q(E_F + E_v) + \Delta E_g^{\mathrm{corr}} + q\Delta V_{av}^{\mathrm{corr}}. \quad (7)$$

Figure 5(a) displays the calculated formation energies of the Fe_{Al} defect with the different net charge q on the Fe impurity with respect to the electronic chemical potential E_F under the oxygen-poor condition. It is shown that the Fe^{3+} ion ($q=0$) is the easiest to form the Fe_{Al} defect for a wide range of E_F. Since the single-crystal growth temperature of KABO is high ($\sim$1100 K), E_F in this environment is located at the midpoint of E_g.[32] The corresponding formation energies of the Fe_{Al} impurity, formed from the Fe ion in various charge states, are shown in Fig. 5(b) as a function of the oxygen chemical potential. One can see that as long as the net charge on the Fe ion differs from zero, the formation energies of the Fe_{Al} impurity significantly increase over whole range of μ_O. The more electrons that are lost or gained on the Fe^{3+} ion, the higher is the corresponding formation energy. Accordingly, the Fe_{Al} impurity concentration c [$\sim\exp(-E_f/k_BT)$] in KABO is greatly reduced. For instance, when Fe^{3+} (E_f =0.32 eV) is ionized to Fe^{2+} (E_f=2.89 eV), its concentration is reduced to $\sim 1/10^{11}$ of the initial value ($\sim$ppm). Consequently, the number of Fe_{Al} ions present in KABO becomes negligible so that the induced UV optical absorption peaks would disappear. Our further electronic structural calculations on the charged Fe_{Al} defect ($q \neq 0$) show the occurrence of the donor states (or the acceptor states), which always makes the system metallic. These metallic states are

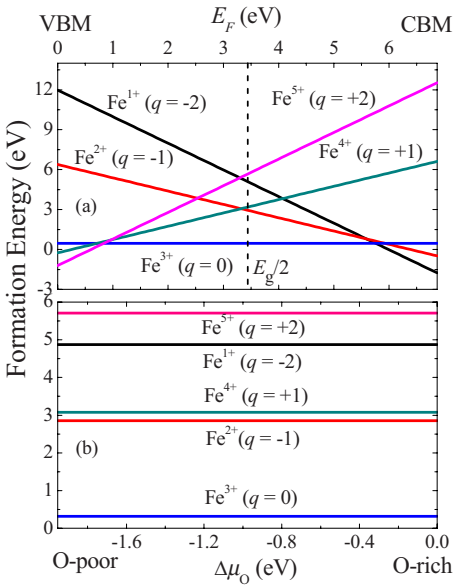

FIG. 5. (Color online) Formation energies of the Fe_{Al} impurity with the different initial net charge q on the Fe impurity (a) as a function of the Fermi level E_F (electron chemical potential) under the oxygen-poor condition and (b) as a function of oxygen chemical potential at $E_F = E_g/2$ [indicated as dashed line in (a)].

less stable compared to the electronic states that possess band gap for the neutral Fe_{Al} defect shown in Fig. 3. This electronic characteristics, therefore, also demonstrates that the Fe_{Al} defect becomes unfavorable as the charge states of the Fe ion are modified. In our experiments, this Fe-impurity engineering consideration has been fulfilled by adopting a special single-crystal growth method in which an oxidized or reduced gas is filled in the growth environment. Since charge states of the Fe ion are much easier to be changed than other elements in KABO, this treatment can effectively modify the charge state of Fe^{3+}, rather than others. This modification indeed prevents the Fe incorporation from the Al site and consequently eliminates the UV absorption peaks.[10]

In addition, it is shown in Fig. 5(a) that the acceptorlike defect ($+q$) becomes more and more stable as E_F decreases, even more stable than the neutral defect when E_F approaches the VBM while the donorlike defect ($-q$) behaves in an opposite manner since its formation energy is lower than the neutral case in the region close to the CBM. This means that E_F can modify the most stable charge state on the impurity ions. Therefore, one might be able to engineer the formation and electronic characteristics of impurities in materials by modifying their charge state (e.g., using our special growth method) and/or the ambient electronic chemical potential (e.g., contacting the material with electrodes), and further improve the material quality.

IV. CONCLUSIONS

In summary, a comprehensive *ab initio* study of iron impurity in KABO has been carried out. It is found that Fe substitution on an Al site is preferred under conditions used in the conventional single-crystal growth method due to its very low formation energy. The electronic transition between the O $2p$ states and the unoccupied Fe_{Al} $3d$ band-gap states split by the crystal-field environment induces the occurrence of UV optical absorption peaks, in very good agreement with the experimental observations, not only for the positions but also for the relative intensity. This optical problem in KABO can be resolved by modifying the charge state of the impurity during crystal growth, which makes the Fe_{Al} defect much more difficult to form in the host since it has much higher energy barrier. The understanding of the optical absorption induced by an impurity and the way it can be suppressed has significant implications for other oxide materials with similar problems.

ACKNOWLEDGMENTS

We thank S. B. Zhang and P. B. Bristowe for useful discussions. This work was supported by the Special Foundation of the President of the Chinese Academy of Sciences and National Basic Research Project (Grant No. 2010CB630701) and National Science Foundation of China (Grants No. 10634070 and No. 10774177) as well as Grant No. NSC 97-2112-M-032-004-MY2 in Taiwan.

[1] D. Cyranoski, Nature (London) **457**, 953 (2009).
[2] N. Umemura, M. Ando, K. Suzuki, E. Takaoka, K. Kato, Z. G. Hu, M. Yoshimura, Y. Mori, and T. Sasaki, Appl. Opt. **42**, 2716 (2003).
[3] C. T. Chen, Laser Focus World **40**, 91 (2004).
[4] Y. K. Yap, M. Inagaki, S. Nakajima, Y. Mori, and T. Sasaki, Opt. Lett. **21**, 1348 (1996).
[5] Y. C. Wu, P. Z. Fu, J. X. Wang, Z. Y. Xu, L. Zhang, Y. F. Kong, and C. T. Chen, Opt. Lett. **22**, 1840 (1997).
[6] K. Kondo, M. Oka, H. Wada, T. Fukui, N. Umezu, K. Tatsuki, and S. Kubota, Opt. Lett. **23**, 195 (1998).
[7] C. T. Chen, G. L. Wang, X. Y. Wang, and Z. Y. Xu, Appl. Phys. B: Lasers Opt. **97**, 9 (2009).
[8] N. Ye, W. Zeng, B. Wu, and C. T. Chen, Proc. SPIE **3556**, 21 (1998).
[9] Z. G. Hu, Y. Mori, T. Higashiama, Y. K. Yap, Y. Kagebayash, and T. Sasaki, Proc. SPIE **3556**, 156 (1998).
[10] L. Liu, C. Liu, X. Wang, Z. G. Hu, R. K. Li, and C. T. Chen, Solid State Sci. **11**, 841 (2009).
[11] G. S. Shao, J. Phys. Chem. C **113**, 6800 (2009).
[12] V. I. Anisimov, M. A. Korotin, J. A. Zaanen, and O. K. Andersen, Phys. Rev. Lett. **68**, 345 (1992).
[13] A. Roldán, M. Boronat, A. Corma, and F. Illas, J. Phys. Chem. C **114**, 6511 (2010).
[14] F. H. ElBatal, Y. M. Hamdy, and S. Y. Marzouk, J. Non-Cryst. Solids **355**, 2439 (2009).
[15] M. C. Payne, M. P. Teter, D. C. Allan, T. A. Arias, and J. D. Joannopoulos, Rev. Mod. Phys. **64**, 1045 (1992).

[16] S. J. Clark, M. D. Segall, C. J. Pickard, P. J. Hasnip, M. J. Probert, K. Refson and M. C. Payne, Z. Kristallogr. **220**, 567 (2005).
[17] D. Vanderbilt, Phys. Rev. B **41**, 7892 (1990).
[18] J. P. Perdew, K. Burke, and M. Ernzerhof, Phys. Rev. Lett. **77**, 3865 (1996).
[19] H. J. Monkhorst and J. D. Pack, Phys. Rev. B **13**, 5188 (1976).
[20] T. H. Fischer and J. Almlof, J. Phys. Chem. **96**, 9768 (1992).
[21] S. B. Zhang, J. Phys.: Condens. Matter **14**, R881 (2002).
[22] C. Q. Zhang, J. Y. Wang, X. B. Hu, H. D. Jiang, Y. G. Liu, and C. T. Chen, J. Cryst. Growth **235**, 1 (2002).
[23] V. I. Anisimov, J. Zaanen, and O. K. Andersen, Phys. Rev. B **44**, 943 (1991).
[24] E. D. Palik, *Handbook of Optical Constants of Solids* (Academic, New York, 1985).
[25] R. W. Godby, M. Schluter, and L. J. Sham, Phys. Rev. B **37**, 10159 (1988).
[26] C. S. Wang and B. M. Klein, Phys. Rev. B **24**, 3417 (1981).
[27] C. T. Chen, Z. S. Lin, and Z. Wang, Appl. Phys. B: Lasers Opt. **80**, 1 (2005).
[28] M. H. Lee, C. H. Yang, and J. H. Jan, Phys. Rev. B **70**, 235110 (2004).
[29] S. Lany and A. Zunger, Phys. Rev. B **78**, 235104 (2008).
[30] G. Makov and M. C. Payne, Phys. Rev. B **51**, 4014 (1995).
[31] C. G. Van de Walle and J. Eugebauer, J. Appl. Phys. **95**, 3851 (2004).
[32] C. Kılıç and A. Zunger, Phys. Rev. Lett. **88**, 095501 (2002).